RSC Advances

ROYAL SOCIETY OF CHEMISTRY

www.rsc.org/advances

Investigation of cobalt redox mediators and effects of TiO_2 film topology in dye-sensitized solar cells

Majid Safdari[§,#], Peter W. Lohse[§], Leif Häggman[§], Sara Frykstrand[¤] , Daniel Högberg[#], Mark Rutland,[&] Rubén Alvarez Asencio,[&,2] James Gardner[#], Lars Kloo[#], Anders Hagfeldt[§], Gerrit Boschloo[§,]*

[#]Applied Physical Chemistry, Center for Molecular Devices, Department of Chemistry, KTH Royal Institute of Technology, SE-100 44, Stockholm, Sweden.

[§]Physical Chemistry, Center for Molecular Devices, Department of Chemistry - Ångström Laboratory, Uppsala University, SE-751 20 Uppsala, Sweden.

[¤]Division for Nanotechnology and Functional Materials, Department of Engineering Sciences, Ångström Laboratory, Uppsala University, Box 534, SE-751 21 Uppsala, Sweden.

[&]Surface and Corrosion Science, Department of Chemistry, KTH Royal Institute of Technology, SE-100 44 Stockholm, Sweden

2) Current Affiliation: Institute for Advanced Studies, IMDEA Nanoscience, c/ Faraday 9, Campus Cantoblanco, 28049 Madrid, Spain

Abstract

One-electron outer-sphere redox couples, such as cobalt metal-organic complexes, represent an interesting alternative as redox mediators in dye-sensitized solar cells since they show weak visible light absorption and available redox potentials may lead to higher open circuit voltage values. Here, we have studied the effect of using different substituents on bipyridyl and phenantroline ligands in cobalt redox shuttles, giving the following complexes: Co[tris(4-

4′-dimethoxy-2-2′-bipyridine)$(PF_6)_2$], Co[tris(4,4'-dichloro-2,2'-bipyridine)$(PF_6)_2$] and Co[tris(4,7-dichloro-1,10-phenanthroline)$(CF_3SO_3)_2$]), displaying a range of CoII/CoIII redox potentials from +0.37 to +0.79 V vs. NHE. The regeneration kinetics of the organic dye D35 was found to depend systematically on the redox mediator potential, which was explained using the Marcus theory. The mass transport of cobalt mediators in dye-sensitized solar cells is highly dependent on the porosity, effective surface area and roughness of the mesoporous TiO_2 films. Therefore, films with different TiO_2 pore sizes were prepared and investigated to get an insight into the topological effects of TiO_2 film preparation in order to obtain optimum solar cell performance.

Keywords: *Dye-sensitized solar cell, cobalt complex, regeneration efficiency, mass transport, porosity.*

1. Introduction

Dye-sensitized solar cells (DSSCs) have attracted much interest after their discovery because of their potential for low cost production, rapid energy payback time and attractive colorful design. DSSCs contain two electrodes, sensitizing molecules and a redox electrolyte as central components. Sunlight is absorbed by the sensitizing dye molecules anchored to a mesoporous, wide-bandgap semiconductor substrate. The excited dyes inject electrons into the conduction band of the substrate semiconductor. The oxidized dye molecules will be regenerated by a redox couple mediator in the electrolyte[1-2]. The first generation of electrolytes in efficient DSSCs contained the iodide/triiodide redox couple, which energetically matches ruthenium-based sensitizing dyes well and have shown up to 11% power conversion efficiency.[3] DSSCs based on iodide/triiodide electrolytes have, however, some limitations. For instance, there is a high overpotential for dye regeneration, which implies a significant loss of photovoltage.[4] There is also competitive light absorption by triiodide ions in the electrolyte shadowing the sensitizing dye molecules, which lower the photocurrent in the solar cell.[2] Due to such limitations alternative redox mediators are desirable to boost conversion efficiencies in DSSCs.

In 2010, Feldt et al. reported an efficient dye-sensitized solar cell containing a cobalt bipyridyl redox mediator in combination with a bulky organic dye with suitable recombination-blocking properties.[5] This has led to a renewed interest in DSSCs based on such mediators in combination with organic[6] and porphyrin dyes[7] showing promising power conversion efficiencies up to 13.0%.[7] In parallel modified cobalt complexes have been studied for example, imidazolium cobalt tris(bipyridyl) complexes redox mediators has been used in combination with ruthenium dye (N719) in dye DSSCs.[8] The main advantage of cobalt redox couples is that a lower overpotential is required for dye regeneration and that higher a photovoltage thus can be obtained. A further advantage is that cobalt redox mediators have

much lower visible light absorption than triiodide ions, which should give also a higher photocurrent. As cobalt bipyridyl redox mediators are one-electron, outer-sphere redox couples, they tend to give shorter electron lifetimes in DSSCs due to a higher charge recombination loss rate, instead leading to an overall decreased power conversion efficiencies.[9-11] It is therefore essential that the dye molecule is based on a structure that inhibits the undesirable electron recombination loss, for instance by hosting multiple and bulky alkoxy groups.[5]

The DSSC represents a complex device system with several electron transfer reactions and interactions that need to be fine-tuned in order to render high conversion efficiencies.[2, 12] The electron transfer reactions need to have an appropriate driving force to give desirable rates, but driving forces should not be excessive as these result in an unwanted energy loss. In order to obtain highly efficient DSSCs the energy levels of different components should therefore be carefully optimized, requiring a rather tedious effort. The redox potential of cobalt complex redox couples can be adjusted by modification of the ligand structure. It has been shown that by tuning the coordination of the cobalt complex open-circuit potentials of more than 1 V can be obtained in combination with a driving force for regeneration of 0.25 V.[6] In the present work we have investigated the effect of altering the ligand structures of the cobalt complexes on the regeneration rates of the dye. The changes to the cobalt ligands were based on the introduction of electron-donating groups, e.g. methoxy substituents, or electron withdrawing groups, e.g. chloride ions, to the bipyridine ligands. These modifications will change the redox potential of the cobalt complex as a whole, and will also affect the electron regeneration efficiencies and overall solar cell performance. the electron transfer kinetics were investigated using laser flash photolysis, and the results were explained using the Marcus theory. As sensitizer, the efficient triphenylamine-based organic dye D35 [((E)-3-(5-

(4-(bis(20,40-dibutoxybiphenyl-4-yl)amino)phenyl) thiophen-2-yl)-2-cyanoacrylic acid] was used.[13]

A series of new cobalt redox couples were examined as redox mediators in the electrolyte of the DSSCs. The cobalt complexes studied were cobalt(II/III) tris (2,2′-bipyridine), cobalt(II/III) tris (4-4′-dimethoxy-2-2′-bipyridine), cobalt (II/III) tris (4,7-dichloro-1,10-phenanthroline), and cobalt (II/III) tris (4,4′-dichloro-2,2'-bipyridine). Furthermore, optimal DSSC performance using cobalt-based electrolytes strongly depend on an optimized TiO_2 film. In comparison to standard DSSCs based on the iodide/triiodide redox system, typically thinner and more porous TiO_2 films are required to render high conversion efficiencies. The standard way to accomplish such changes to the TiO_2 film is to dilute an ordinary TiO_2 paste using ethylcellulose and terpineol or similar agents. It is expected that such a dilution will lead to a more porous TiO_2 topology allowing more efficient diffusion of the comparably large cobalt complexes within the mesoporous film. The strategy obviously works, but as will be shown in this study, the effects of TiO_2 paste dilution and $TiCl_4$ treatment are a bit more complex than presumed, involving both changes in surface area, roughness as well as crack formation.

2. Experimental Section

All chemicals were purchased from Sigma Aldrich unless specifically noted. Synthesis of cobalt complexes was done according to a procedure described elsewhere. D35 was synthesized according to the published procedure.[13] The 4,4'-dichloro-2,2'-bipyridine (dclbpy) ligand was purchased from HetCat (Basel, Switzerland).

2.1. Synthesis of cobalt complexes. Cobalt complexes were synthesized according to a previously published procedure.[9, 14] For the synthesis of $Co(bpy)_3(PF_6)_2$, $Co(dclbpy)_3(PF_6)_2$, and $Co(dclphen)_3(CF_3SO_3)_2$, one equivalent of $CoCl_2 \cdot 6\ H_2O$ was dissolved in a minimal

amount of methanol and added to a solution containing 3.3 equivalents of the ligand dissolved in methanol. This mixture was stirred under reflux for 2 hours. An oil bath was used to adjust the temperature to 90 °C. For precipitation of the product, 3 equivalents of tetra-butylammonium hexafluorophosphate powder was added to the solution. In the case of $Co(dclphen)_3(CF_3SO_3)_2$, instead 3 equivalents of lithium trifluoromethanesulfonate powder was added to the solution. The product was precipitated in this step, but addition of excess amount of diethyl ether may be required. The product was filtered, washed with ethanol and dried under vacuum. The trifluoromethanesulfonate counterion in $Co(dclphen)_3(CF_3SO_3)_2$ renders a higher solubility of the cobalt complex in common polar solvents. The ligand 4-4′-dimethoxy-2-2′-bipyridine is only sparingly soluble in methanol, and consequently another procedure was used for the synthesis of the related complex[15]. Two equivalents of this ligand were instead dissolved in dichloromethane. Then, one equivalent of $CoCl_2$ was added to this solution. This mixture was stirred under reflux for 5 hours. An oil bath (90 °C) was used to adjust the temperature. Although $CoCl_2$ is not highly soluble in dichloromethane, the product is soluble and as the reaction proceeds $CoCl_2$ was completely dissolved and the product was obtained as a pink solution. Further reaction was performed under reflux in order to get the three-coordinated cobalt complex. One equivalent of $Co(ligand)_2Cl_2$ was dissolved in ethanol, and one further equivalent of ligand was added to this solution. The reaction was completed under reflux for 1 hour. Three equivalents of tetrabutylammonium hexafluorophosphate ($[TBA]PF_6$) were added to precipitate the product, which was filtered and dried under vacuum. Oxidation of cobalt complexes was performed by adding 3.3 equivalents of $[NO]BF_4$ to an acetonitrile solution of the corresponding cobalt(II) complex. The solvent was removed by using a rotatory evaporator. The complex was dissolved in acetonitrile again and 3.3 equivalents of $[TBA]PF_6$ powder was added. Finally, the complex compound was precipitated

by addition of diethyl ether. The product was filtered and dried under vacuum. The molecular structures of the cobalt complexes synthesized are shown in Figure 1.

2.2. Solar cell fabrication. Fluorine-doped tin oxide substrates (FTO-Pilkington, TEC 15) were cleaned by washing with detergent in an ultrasonic bath for 30 min. followed by cleaning with water, and ethanol in ultrasonic bath for one hour. FTO substrates were pretreated in 40mM $TiCl_4$ aqueous solution at 70ºC for 90 minutes, then rinsed with water and ethanol. Mesoporous TiO_2 films with area of 0.25 cm^2 were prepared by screen-printing.

Three different transparent pastes of TiO_2 were used: Paste A, Dyesol 18NR-T (batch 300); Paste B, a mixture of 60 wt% of Dyesol 18NR-T and a mixture of 4 wt% ethylcellulose and 36 wt% terpineol; Paste C, 40 wt% of Dyesol 18NR-T, 6 wt% ethylcellulose and 54 wt% terpineol. The Dyesol paste PST-400c was used as a scattering paste. The mesh size of the printing screen was 53T. After printing, the electrodes were allowed to rest for 15 minutes in an ethanol atmosphere and were then dried at 125 ºC for 6 minutes. For thicker layers, screen-printing was repeated several times. The electrodes were heated to 325ºC for 5 minutes and further to 450 ºC for 30 minutes using an oven. Finally, the electrodes were immersed into a 40mM $TiCl_4$ aqueous solution at 70ºC for 45 minutes and re-sintered at 450ºC for 30 minutes.

After sintering, when the temperature reached 90 ºC, dye sensitization was performed in a solution of 0.2mM D35 in ethanol for 16 hours. Platinized counter electrodes were prepared by deposition of 10 μL cm^{-2} of 4.8 mM H_2PtCl_6 in ethanol followed by heating at 400 ºC for 30 min. The D35-sensitized working electrodes were washed with ethanol and dried in vacuum. Fabrication of solar cells was performed using a sealing machine (DHS-ES2-35, Heptachroma Solar Technologies) by a 25 μm thick Surlyn thermoplastic frame (internal size 7 mm × 7 mm). The working electrode, thermoplastic frame, and the counter electrode were joined in a sandwich configuration. Electrolyte solutions used consisted of 0.22 M Co^{II}

complex, 0.05 M of Co^{III} complex, 0.1 M $LiClO_4$ and 0.2 M TBP (4-tert-butylpyridine) in a mixture of 40 wt% ethylene carbonate + 60 wt% acetonitrile. This solvent mixture was chosen because of the low solubility of cobalt tris(4,7-dichloro-1,10-phenanthroline)$(CF_3SO_3)_2$ in acetonitrile.

2.3. Nitrogen sorption measurements. Nitrogen sorption measurements were carried out at 77 K using an ASAP 2020 apparatus from Micromeritics. The samples were degassed at 100 °C for 10 h prior to analysis with a vacuum set-point of 10 μm Hg. The specific surface area (SSA) was determined by applying the Brunauer–Emmet–Teller (BET) equation[16] to the relative pressure range 0.05–0.30 of the adsorption branch of the isotherm. The pore size distributions were determined according to the Barrett-Joyner-Halenda (BJH) method[17] during desorption.

2.4. Electrochemical and optical Analyses. Cyclic voltammetry was performed using A CH instrument 660 potentiostat. A platinum microelectrode (20 μm diameter) was used as working electrode, a platinum wire (1.0 mm diameter, 99.9% metal basis) as counter electrode and an electrode with non-aqueous solution of Ag/Ag^+ (0.01 M $AgNO_3$, 0.1 M $[TBA]PF_6$ in acetonitrile) as reference electrode. The redox solution contained the cobalt complex (15 mM) and $[TBA]PF_6$ (0.1 M). Cyclic voltammetry measurements were performed at 10 mVs^{-1} scan rate. A solution of 15 mM ferrocene and 0.1 M $[TBA]PF_6$ was used for calibration.

Light absorption measurements were performed using an HR-2000 Ocean Optics fiber optics spectrophotometer. Calibration was done against air before start of the experiments. A solution of 15 mM of each mediator and a 1 mm quartz cuvette were used for this experiment.

Transient absorption spectroscopy (TAS) measurements were performed at room temperature (21-22 ºC) using an Edinburgh Instrument LP920 laser flash photolysis spectrometer. Laser pulses were generated by a frequency tripled Nd:YAG laser (Continuum Surelight II, 10 Hz

repetition rate, 10 ns pulse width) in combination with an optical parametric oscillator (OPO) (Continuum Surelight), tuned to 560

nm. The absorption spectra of the excited samples were recorded with a near-infrared LED (Osram SHF 484, λ_{max} 880 nm, FWHM 80 nm) as probe light and an amplified Si photodiode (Thorlabs PMA10A) as detector. Doctor-bladed TiO_2 films were prepared with diluted TiO_2 paste (60 wt% Dyesol 18-NR-T + 40 wt% isopropanol) on microscope glass substrates followed by heating at 450 ºC. The thickness of the prepared films was around 4 μm. Sensitization was performed in a 0.2 mM solution of D35 for 90 min. A solvent of 40 wt% ethylene carbonate and 60 wt% acetonitrile was used for the cobalt-containing electrolyte solutions. A solution of 0.22 M Co^{II} of each complex, 0.2 M TBP and 0.1 M $LiClO_4$ was used in the measurements. After excitation by the Nd:YAG laser at 530 nm, transient absorption measurements were performed at 880 nm, where the oxidized dye shows a significant absorbance. Measurements using an inert electrolyte (0.2 M TBP and 0.1 M $LiClO_4$ in a mixture of 40 wt% ethylene carbonate and 60 wt% acetonitrile) were used to determine the recombination rates.

Current−voltage (I−V) characteristics of the solar cells were recorded using a Keithley 2400 source/meter and a Newport solar simulator (model 91160) giving light with AM 1.5 G spectral distribution, which was calibrated using a certified reference solar cell (Fraunhofer ISE) to an intensity 1000 W m^{-2}, or with the help of a neutral density filter to 100 W m^{-2}. The measurements were performed at room temperature (21-22 ºC).

Incident photon to current conversion efficiency (IPCE) spectra were recorded using a computer-controlled setup consisting of a xenon light source (Spectral Products ASB-XE-175), a monochromator (Spectral Products CM110), and a Keithley multimeter (model 2700), calibrated using a certified reference solar cell (Fraunhofer ISE). Electron lifetime, transport

times, and extracted charge measurements were performed using a white LED (Luxeon Star 1W) as light source. Voltage and current traces were recorded with a 16-bit resolution digital acquisition board (National Instruments) in combination with a current amplifier (Stanford Research Systems SR570) and a custom-made system using electromagnetic switches. Transport and lifetimes were determined by monitoring photocurrent and photovoltage transients at different light intensities upon applying a small square wave modulation to the base light intensity. The photocurrent and photovoltaic responses were fitted using first-order kinetics in order to obtain time constants.[18]

2.5 **AFM Analysis.**

AFM images were collected by using a Bruker Dimension Icon (Bruker Nanosurfaces, CA) located in the AlbaNova Nanofabrication Facility (Stockholm, Sweden) in tapping mode using: a). Si tips coated by 20 nm DLC (diamond like carbon) (HQNSC35_HARD_ALBS, MikroMasch, Tallinn, Estonia, with a nominal normal spring constant of 5.4 N/m); b) Ultrasharp Si tips (HQNSC15_ALBS, MikroMasch, Tallinn, Estonia, with a nominal normal spring constant of 40 N/m).

Before imaging, the surfaces were cleaned by thorough rinsing with ethanol, followed by drying using N_2 gas. Processing of the obtained AFM images and the calculation of their *R*q roughness were performed by using the AFM software (Nanoscope 6.13R1).

3. Results and discussion

3.1. Mesoporous TiO_2 electrodes for cobalt based dye-sensitized solar cells. Mesoporous TiO_2 films prepared using the different pastes were analyzed by N_2 gas adsorption/desorption

experiments. A summary of the results is shown in Table 1. The porosity of the standard mesoporous TiO_2 films prepared from the Dyesol 18NR-T paste, having an average particle size of 20 nm, was determined to be 64%. An after-treatment based on aqueous $TiCl_4$ is frequently used on this type of films in order to improve the performance in DSSCs.[18,19] The effect of this treatment is a significant reduction of the porosity to 58%, while the BET surface area increased from 62 to 67 m^2g^{-1}. These results are in accordance with previous investigations of the $TiCl_4$ treatment effect, and are explained by the deposition of small TiO_2 nanoparticles on the internal surface of the mesoporous TiO_2 film.[19,19] It is also notable that the so-called skewness of the TiO_2 film surface changes from negative values (indicating a topology dominated by valleys) to positive values (indicating a topology dominated by peaks) upon the $TiCl_4$ treatment. The decrease in porosity caused by the $TiCl_4$ treatment is expected to be a disadvantage for the use in DSSCs in combination with cobalt-based electrolytes considering the molecular size of the cobalt redox couple complexes. As noted above, the typical way to render a more porous TiO_2 film is to dilute the TiO_2 using for instance ethylcellulose.[20-21] The addition of ethylcellulose to the commercially available TiO_2 paste (Paste A), giving Paste B and C, resulted in mesoporous films with significantly higher surface area (by up to 30% higher) and somewhat higher porosity (up to 10% higher). It is also notable that in addition to an increase in porosity and surface area, dilution also leads to significant cracking in the films. Cracks formed are typically a few micrometers wide and form a complex and extended pattern with a typical distance between cracks of 10-20 micrometers (see Figure 2; cf. non-diluted paste in Figure S5). The dilution of the TiO_2 paste gives clear macroscopic effects (changing the roughness and the density of cracks) rather than on the microscopic effect (changing the porosity). It is likely that these cracks also contribute to the porosity and roughness determined, as well as to the overall effective cobalt complex diffusion in the TiO_2 films. Although we did not study the effect of $TiCl_4$ treatment of films

prepared from the Pastes B and C, we can assume that such as treatment will lead to a similar reduction of porosity. Figure 3 shows the pore size distribution of the different mesoporous films. A clear effect is the widening of the pores by addition of extra ethylcellulose to the TiO_2 screen printing paste. Films prepared from Paste C show the largest porosity, and exhibit the largest pores with a diameter centered of approximately 28 nm (see Figure 3), while the other samples have approximately the same pore diameter of approximately 20 nm. It is also clear from the pore-size distributions that the Paste A films after $TiCl_4$ treatment display a smaller pore volume than the others, which is in agreement with the lower porosity noted for that type of film. As noted above, also surface roughness and cracks are likely influence the overall performance of the DSSCs, thus linking the observed photovoltaic effects both to microscopic and macroscopic origin of the titania film morphology.

Figure 4 shows two images obtained from the AFM measurements, which gives a visual representation of the individual nanoparticles of the TiO_2 electrodes (Paste A) and their configuration. It appears that smaller sized nanoparticles are present in the sample treated with $TiCl_4$ (bottom image) as compared to the untreated sample (top image). The AFM images suggest that after treatment of TiO_2 electrode by $TiCl_4$ solution small particles of TiO_2 are formed on the surface of TiO_2 electrodes. This appears to be the main reason for the increase in specific surface area after $TiCl_4$ treatment. [19, 22]

The solar cell performance of the different TiO_2 films with various film thicknesses was also investigated (see Supporting Information), and Paste B was found to yield the best performance in the DSSCs studied in combination with cobalt-based electrolytes. This paste with the optimized thickness was used for the remainder of this study.

3.2.Cobalt-based redox mediators for dye-sensitized solar cells. UV-visible spectra of the cobalt complexes synthesized were recorded and their extinction coefficients were estimated

using the Beer Lambert relation. Spectra are presented in Figure S1 in the Supplementary Information. For $[Co(dMeObpy)_3]^{2+}$, $[Co(dclbpy)_3]^{2+}$, $[Co(dclphen)_3]^{2+}$ and $[Co(bpy)_3]^{2+}$ calculated extinction coefficients at 480 nm are 73 $M^{-1}cm^{-1}$, 60 $M^{-1}cm^{-1}$, 40 $M^{-1}cm^{-1}$, 43 $M^{-1}cm^{-1}$, respectively. Cyclic voltammetry (Figure S2 in Supplementary Information) of 15mM acetonitrile solutions of the complexes were evaluated and their redox potential values were obtained. For $[Co(bpy)_3]^{2+/3+}$ a value of 0.56 V vs. the Normal Hydrogen Electrode (NHE) was determined. Addition of electron-donating methoxy groups to the bpy ligand in ($[Co(dMeObpy)_3]^{2+/3+}$) shifts the $E^{0'}$ to a less positive potential (0.37 V vs. NHE), while the electron-withdrawing chloride substituent ($[Co(dclbpy)_3]^{2+/3+}$) instead shifts the redox potential to a more positive potential (0.79 V vs. NHE). Finally, for $[Co(dclphen)_3]^{2+73+}$ the redox potential obtained is 0.77 V vs. NHE, which may be compared to the non-substituted cobalt tris(phenanthroline) value of 0.62 V.[5]

Nanosecond transient absorption measurement experiments were performed in order to determine the effect of the different redox potentials of the cobalt redox couples on the rate of regeneration of the D35 dye. The decay in absorbance of an inert solution was evaluated in order to allow evaluation of the recombination kinetics and decay in absorbance for each redox system. Regeneration efficiencies were calculated using equation 1.[23]

$$\phi_{reg} = \frac{k_{reg}}{k_{reg}+k_{rec}} = 1 - \frac{\tau_{\frac{1}{2}redox}}{\tau_{\frac{1}{2}inert}} \qquad (1)$$

where k_{rec} is the rate constant for recombination of an injected electron in the TiO_2 conduction band with the oxidized dye, k_{reg} is the rate constant of regeneration of the oxidized dye by the reduced component of the redox system in the electrolyte, $\tau_{1/2redox}$ is the halftime observed in the presence of the redox electrolyte $\tau_{1/2inert}$ the halftime observed in the presence of the inert electrolyte.

The halftime of the recombination of photoinjected electrons from the titania conduction band with the oxidized D35 dye was determined to be 320 μs, see Figure 5. The absorbance signal, which is attributed to the electrons in TiO_2, was subtracted from the transient absorption signal in order to calculate regeneration time constant. Regeneration halftimes and regeneration efficiencies are presented in Table 2. For the cobalt redox species the obtained regeneration half times were 5.2±0.04, 6.6±0.1, 28.4±0.1 and 40.1±1.0 μs for $Co^{II}(bpy)_3$, $Co^{II}(dMeO\text{-}bpy)_3$, $Co^{II}(dclbpy)_3$, $Co^{II}(dclphen)_3$, respectively. The shortest regeneration halftime is observed for $Co^{II}(bpy)_3$ suggesting a very rapid regeneration of the oxidized dye by the electrolyte species. The longer regeneration halftime for $Co^{II}(dclphen)_3$ could be explained by the more positive redox potential and weaker electronic coupling due to the increase in steric bulk of $Co^{II}(dclphen)_3$.

The electron transfer kinetics in DSSCs are expected to be properly described by the Marcus theory for electron transfer in a homogeneous medium.[24-25] The rate constant of electron transfer is given by equation 2. ΔG° is the free energy needed for the reaction, H_{AB}^2 is the electronic coupling between donor and acceptor and λ is the reorganization energy, and these are the parameters that govern electron transfer kinetics according to the theory. The structure of both of the dye and the redox mediator are very important factors that affect the rate of electron transfer, since both the donor and acceptor will influence the reorganization energy as well as the electronic coupling.[25]

$$k_{et} = \frac{H_{AB}^2}{\sqrt{4\pi\lambda k_B T}} exp\left(\frac{(\Delta G^0+\lambda)^2}{4\lambda k_B T}\right) \quad (2)$$ [25]

The estimated regeneration efficiencies of 98% for the $Co^{II}(bpy)_3$ and $Co^{II}(dMeO\text{-}bpy)_3$ complexes indicate that the regeneration of the oxidized dye by these mediators is sufficiently fast to not represent a bottleneck in the DSSC photovoltaic processes.

It is expected that in the normal region of the Marcus theory the rate of electron transfer is increased by an increase in the ΔG^0 value. This can be confirmed using the calculated regeneration efficiency for $Co^{II}(bpy)_3$, $Co^{II}(dclbpy)_3$ and $Co^{II}(dclphen)_3$. According to the Marcus theory, the highest possible regeneration efficiency could be attributed to the situation where the driving force is equal to the reorganization energy. The inverse of the obtained regeneration halftimes are shown in a semilogaritmic plot in Figure 6, including a fit of Eq. 2. The obtained reorganization energy is 0.65 eV (i.e., the maximum of the fitted curve), which is agreement with our previous regeneration studies on cobalt redox mediators and D35.[23]

D35-sensitized solar cells were fabricated using these cobalt mediators in order to investigate the effect of different driving forces and regeneration efficiencies on the photovoltaic performance. A mixture of 40 wt% ethylene carbonate + 60 wt% acetonitrile was used as solvent for the electrolyte. The choice of electrolyte solvent was mainly caused by the solubility problems for $Co^{II/III}(dclphen)_3$ in pure acetonitrile. The best performance was obtained for solar cells containing the $Co^{II/III}(bpy)_3$ redox couple with an open-circuit potential (V_{OC}) of 0.85 V, a current density of 9.85 mA cm^{-2}, a fill factor of 0.70 and a total conversion efficiency of 5.8%. The performance of this solar cell is slightly lower than that based on pure acetonitrile as electrolyte solvent (6.5%), which can be attributed to the higher viscosity of the mixed solvent electrolyte resulting in a restricted mass transport of the redox mediator and consequently a lower current density of the cell. For the $Co^{II}(dclbpy)_3$-based solar cells 4.0 % power conversion efficiency was obtained. Higher performance may be expected for solar cells based on acetonitrile as solvent for the electrolyte and after further optimization. IV and IPCE characterization data are presented in Figure 7 and Table 3. Since the open-circuit potential is given by the difference of the Fermi-level in the TiO_2 and the redox potential of the electrolyte, it increases with the redox potential of the mediator as expected. $Co^{II/III}(dclphen)_3$ slightly deviates from this trend with a lower V_{OC} than predicted due to

relatively fast recombination, as will be discussed later. Maximum IPCE values of 90% were obtained for solar cells based on $Co^{II}(bpy)_3$ as mediator. For DSSCs based on $Co^{II}(dclbpy)_3$ IPCE values as high as 88% were obtained. The maximum IPCE value for DSSCs containing $Co^{II}(dMeObpy)_3$ as redox system was relatively low (~70%), in agreement with the lower short-circuit current density values found for the solar cells. The reason for these low values must be attributed to electron recombination losses to the electrolyte during transport in the mesoporous TiO_2, since the regeneration efficiency was determined to be quite high (98%). $Co^{II/III}(dclphen)_3$ had even lower IPCE values due to severe recombination losses.

Electron lifetime and transport time measurements were performed on the solar cells using small-modulation photovoltage/photocurrent methods at a range of incident light intensities. In Figure 8, the electron lifetime is plotted as function of the quasi-Fermi level in TiO_2 for the different solar cells. The unit of the abscissa was chosen in order to account for the differences in redox potential of the different cobalt-based redox electrolytes. As the different redox mediators are not expected to affect the TiO_2 conduction band energy level nor its trap states, essentially the same quasi-Fermi level is expected for states with equal electron concentration in the mesoporous TiO_2 film. The shortest electron lifetimes were obtained using the $Co^{II/III}(dclphen)_3$ system, followed by the $Co^{II/III}(dclbpy)_3$, $Co^{II/III}(dMeO\text{-}bpy)_3$, and finally $Co^{II/III}(bpy)_3$ systems. A higher recombination loss rate was thus obtained for the cobalt-based systems with the most positive redox potential, corresponding to the highest driving force for electron transfer. This suggests that electron transfer takes place in the normal region of the Marcus theory. The electron transport time in the mesoporous TiO_2 was not affected by the presence of different redox couples (see Figure S3). The lower short-circuit photocurrents obtained for DSSCs containing $[Co(dclbpy)_3]^{3+/2+}$, $[Co(dclphen)_3]^{3+/2+}$ and $Co^{II/III}(dMeO\text{-}bpy)_3$, as compared to those containing $[Co(bpy)_3]^{3+/2+}$, can be attributed to the low dye regeneration efficiencies and low charge-collection efficiencies. For the two

chloride-substituted mediators the lower regeneration efficiency accounts for about 10% of the loss in photocurrent. This suggests that the larger part of photocurrent loss is caused by losses in charge collection. It is at this point not clear why the use of $Co^{II/III}(dMeO\text{-}bpy)_3$ leads relatively large charge-collection losses.

Conclusions

Cobalt bipyridine complexes are of interest as alternative as redox mediators in DSSCs. By introduction of electron-donating or -withdrawing groups to the bipyridyl ligands of the complexes, the Co^{II}/Co^{III} redox potential was shifted between +0.37 to +0.79 V vs. NHE in this work. The electron transfer kinetics in D35-sensitized TiO_2 solar cells were investigated and could be explained using the Marcus theory. Regeneration efficiencies of 98% were obtained for electrolytes based on $Co^{II}(dMeO\text{-}bpy)_3$ and $Co^{II}(bpy)_3$. The mass transport of cobalt mediators in DSSCs is highly dependent on the porosity, as well as surface roughness and cracking density, of the mesoporous TiO_2 films. The topological effects were monitored using BET and AFM. Post-treatment using $TiCl_4$ reduces porosity but at the same time increases the surface area, where the latter effects appears to overweigh the former with respect to DSSC performance. The topology of the TiO_2 films was changed by dilution using ethylcellulose added to the screen printing paste and thus to optimize the solar cell performance.

Acknowledgements

This work was supported by the European Community's Seventh Framework Programme (FP7/2007-2013) under grant agreement n° 246124 of the SANS project, the Swedish Energy Agency, the Swedish Research Council (VR), and the STandUP for Energy program

Corresponding Author

* Gerrit Boschloo, gerrit.boschloo@kemi.uu.se

Notes

The authors declare no competing financial interest.

References

(1).O'Regan, B.; Gratzel, M., A low-cost, high-efficiency solar cell based on dye-sensitized colloidal TiO2 films. *Nature* **1991,** *353* (6346), 737-740.
(2).Hagfeldt, A.; Boschloo, G.; Sun, L.; Kloo, L.; Pettersson, H., Dye-Sensitized Solar Cells. *Chemical Reviews* **2010,** *110* (11), 6595-6663.
(3).Chiba, Y.; Islam, A.; Watanabe, Y.; Komiya, R.; Koide, N.; Han, L., Dye-Sensitized Solar Cells with Conversion Efficiency of 11.1%. *Japanese Journal of Applied Physics 45* (21), L638.
(4).Boschloo, G.; Hagfeldt, A., Characteristics of the Iodide/Triiodide Redox Mediator in Dye-Sensitized Solar Cells. *Accounts of Chemical Research* **2009,** *42* (11), 1819-1826.
(5).Feldt, S. M.; Gibson, E. A.; Gabrielsson, E.; Sun, L.; Boschloo, G.; Hagfeldt, A., Design of Organic Dyes and Cobalt Polypyridine Redox Mediators for High-Efficiency Dye-Sensitized Solar Cells. *Journal of the American Chemical Society* **2010,** *132* (46), 16714-16724.
(6).Yum, J.-H.; Baranoff, E.; Kessler, F.; Moehl, T.; Ahmad, S.; Bessho, T.; Marchioro, A.; Ghadiri, E.; Moser, J.-E.; Yi, C.; Nazeeruddin, M. K.; Grätzel, M., A cobalt complex redox shuttle for dye-sensitized solar cells with high open-circuit potentials. *Nat Commun* **2012,** *3*, 631.
(7).Yella, A.; Lee, H.-W.; Tsao, H. N.; Yi, C.; Chandiran, A. K.; Nazeeruddin, M. K.; Diau, E. W.-G.; Yeh, C.-Y.; Zakeeruddin, S. M.; Grätzel, M., Porphyrin-Sensitized Solar Cells with Cobalt (II/III)–Based Redox Electrolyte Exceed 12 Percent Efficiency. *Science* **2011,** *334* (6056), 629-634.
(8).Xu, D.; Zhang, H.; Chen, X.; Yan, F., Imidazolium functionalized cobalt tris(bipyridyl) complex redox shuttles for high efficiency ionic liquid electrolyte dye-sensitized solar cells. *Journal of Materials Chemistry A* **2013,** *1* (38), 11933-11941.
(9).Klahr, B. M.; Hamann, T. W., Performance Enhancement and Limitations of Cobalt Bipyridyl Redox Shuttles in Dye-Sensitized Solar Cells. *The Journal of Physical Chemistry C* **2009,** *113* (31), 14040-14045.
(10).Daeneke, T.; Kwon, T.-H.; Holmes, A. B.; Duffy, N. W.; Bach, U.; Spiccia, L., High-efficiency dye-sensitized solar cells with ferrocene-based electrolytes. *Nat Chem* **2011,** *3* (3), 211-215.
(11).Wang, M.; Chamberland, N.; Breau, L.; Moser, J.-E.; Humphry-Baker, R.; Marsan, B.; Zakeeruddin, S. M.; Grätzel, M., An organic redox electrolyte to rival triiodide/iodide in dye-sensitized solar cells. *Nat Chem* **2010,** *2* (5), 385-389.

(12).Grätzel, M., Solar Energy Conversion by Dye-Sensitized Photovoltaic Cells. *Inorganic Chemistry* **2005,** *44* (20), 6841-6851.
(13).Hagberg, D. P.; Jiang, X.; Gabrielsson, E.; Linder, M.; Marinado, T.; Brinck, T.; Hagfeldt, A.; Sun, L., Symmetric and unsymmetric donor functionalization. comparing structural and spectral benefits of chromophores for dye-sensitized solar cells. *Journal of Materials Chemistry* **2009,** *19* (39), 7232-7238.
(14).Sapp, S. A.; Elliott, C. M.; Contado, C.; Caramori, S.; Bignozzi, C. A., Substituted Polypyridine Complexes of Cobalt(II/III) as Efficient Electron-Transfer Mediators in Dye-Sensitized Solar Cells. *Journal of the American Chemical Society* **2002,** *124* (37), 11215-11222.
(15).Reddy, K. L.; Kumar Reddy, Y. H.; Kumar, K. A.; Vidhisha, S.; Satyanarayana, S., Synthesis, Characterization, DNA-Binding, and DNA-Photocleavage Properties of [Co(bpy)2(7-NO2-dppz)]3+, [Co(dmb)2(7-NO2-dppz)]3+, and [Co(phen)2(7-NO2-dppz)]3+ Complexes: (7-Nitro-dppz = 7-Nitro dipyrido[3,2-a:2′-3′-c]phenazine; bpy = 2,2′-bipyridine; dmb = 4,4′-dimethyl-2,2′-bipyridine; phen = 1,10-phenanthroline) and their Toxicity on Different Microorganisms. *Nucleosides, Nucleotides and Nucleic Acids* **2009,** *28* (3), 204-219.
(16).Brunauer, S.; Emmett, P. H.; Teller, E., Adsorption of Gases in Multimolecular Layers. *Journal of the American Chemical Society* **1938,** *60* (2), 309-319.
(17).Barrett, E. P.; Joyner, L. G.; Halenda, P. P., The Determination of Pore Volume and Area Distributions in Porous Substances. I. Computations from Nitrogen Isotherms. *Journal of the American Chemical Society* **1951,** *73* (1), 373-380.
(18).Boschloo, G.; Häggman, L.; Hagfeldt, A., Quantification of the Effect of 4-tert-Butylpyridine Addition to I-/I3- Redox Electrolytes in Dye-Sensitized Nanostructured TiO2 Solar Cells. *The Journal of Physical Chemistry B* **2006,** *110* (26), 13144-13150.
(19).Ito, S.; Liska, P.; Comte, P.; Charvet, R.; Pechy, P.; Bach, U.; Schmidt-Mende, L.; Zakeeruddin, S. M.; Kay, A.; Nazeeruddin, M. K.; Gratzel, M., Control of dark current in photoelectrochemical (TiO2/I--I3-) and dye-sensitized solar cells. *Chemical Communications* **2005,** (34), 4351-4353.
(20).Kim, H.-S.; Ko, S.-B.; Jang, I.-H.; Park, N.-G., Improvement of mass transport of the [Co(bpy)3]II/IIIredox couple by controlling nanostructure of TiO2 films in dye-sensitized solar cells. *Chemical Communications* **2011,** *47* (47), 12637-12639.
(21).van de Lagemaat, J.; Benkstein, K. D.; Frank, A. J., Relation between Particle Coordination Number and Porosity in Nanoparticle Films: Implications to Dye-Sensitized Solar Cells. *The Journal of Physical Chemistry B* **2001,** *105* (50), 12433-12436.
(22).Sommeling, P. M.; O'Regan, B. C.; Haswell, R. R.; Smit, H. J. P.; Bakker, N. J.; Smits, J. J. T.; Kroon, J. M.; van Roosmalen, J. A. M., Influence of a TiCl4 Post-Treatment on Nanocrystalline TiO2 Films in Dye-Sensitized Solar Cells. *The Journal of Physical Chemistry B* **2006,** *110* (39), 19191-19197.
(23).Feldt, S. M.; Wang, G.; Boschloo, G.; Hagfeldt, A., Effects of Driving Forces for Recombination and Regeneration on the Photovoltaic Performance of Dye-Sensitized Solar Cells using Cobalt Polypyridine Redox Couples. *The Journal of Physical Chemistry C* **2011,** *115* (43), 21500-21507.
(24).Feldt, S. M.; Lohse, P. W.; Kessler, F.; Nazeeruddin, M. K.; Gratzel, M.; Boschloo, G.; Hagfeldt, A., Regeneration and recombination kinetics in cobalt polypyridine based dye-sensitized solar cells, explained using Marcus theory. *Physical Chemistry Chemical Physics* **2013,** *15* (19), 7087-7097.
(25).Pijpers, J. J. H.; Ulbricht, R.; Derossi, S.; Reek, J. N. H.; Bonn, M., Picosecond Electron Injection Dynamics in Dye-Sensitized Oxides in the Presence of Electrolyte. *The Journal of Physical Chemistry C* **2011,** *115* (5), 2578-2584.

Table 1. Results from N_2-gas adsorption (BET) on mesoporous TiO_2 films prepared by different procedures.

Paste	BET Area (m^2 g^{-1})	Porosity(%)
Paste A	61.8	64.4
Paste A + $TiCl_4$ treatment	67.2	58.4
Paste B	78.1	66.0
Paste C	79.5	70.8

Table 2. Regeneration halftimes and regeneration efficiencies for D35-sensitized DSSCs using different cobalt-based redox systems.

Electrolyte	$E^{0'}$ / V vs NHE	$t_{1/2}$ / μs	ϕ_{reg} (%)
Inert	-	320 ± 8	
$Co^{II}(dMeO\text{-}bpy)_3$	0.37	6.6 ±0.1	98
$Co^{II}(bpy)_3$	0.56	5.2 ± 0.4	98
$Co^{II}(dclphen)_3$	0.77	40.1 ± 1.0	87
$Co^{II}(dclbpy)_3$	0.79	28.4 ± 0.1	91

Table 3. Data from IV measurements of D35-sensitized solar cells using different cobalt-based redox mediators.

Cobalt Complex	V_{oc} / V	J_{sc}/mAcm^{-2}	FF	η / %
$[Co(bpy)_3]^{3+/2+}$(MeCN)	0.85	10.8	0.71	6.5
$[Co(bpy)_3]^{3+/2}$	0.850	9.9	0.70	5.8
$[Co(dMeObpy)_3]^{3+/2+}$	0.595	5.2	0.51	1.6
$[Co(dclbpy)_3]^{3+/2+}$	0.940	6.2	0.68	4.0
$[Co(dclphen)_3]^{3+/2+}$	0.780	2.0	0.68	1.1

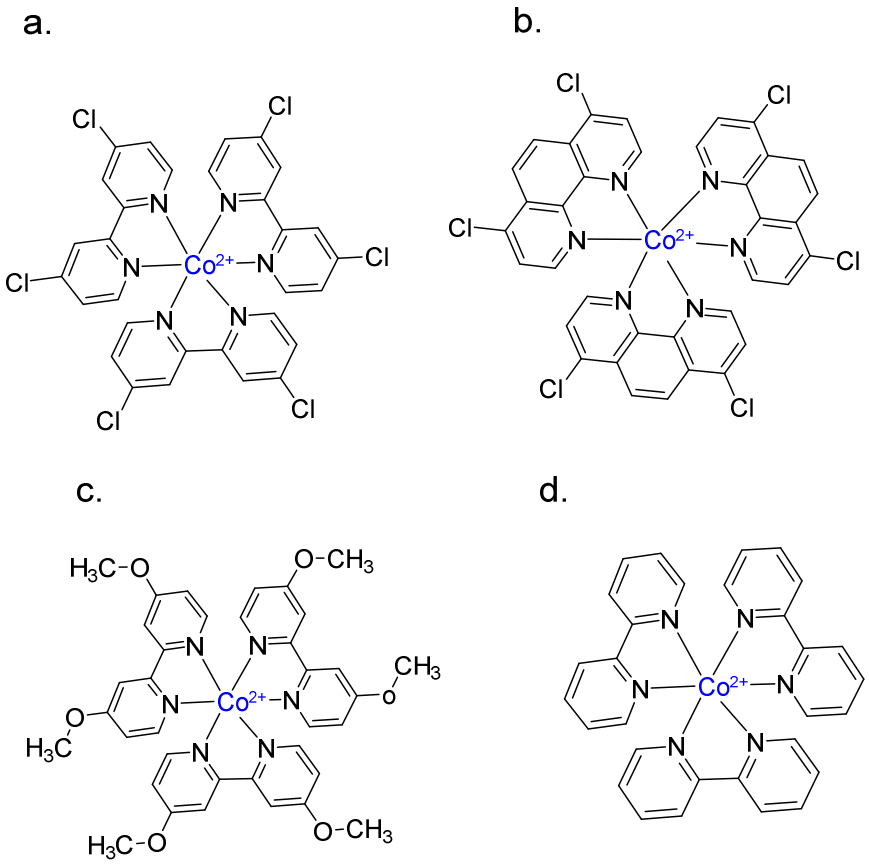

Figure 1. Molecular structures of a) [cobalt^{II} tris (4,4'-dichloro-2,2'-bipyridine)]; b) [cobalt^{II} tris(4,7-dichloro-1,10-phenanthroline)]); c) [cobalt^{II} tris(4-4′-dimethoxy-2-2′-bipyridine)] and d) [cobalt^{II} tris(bipyridine)].

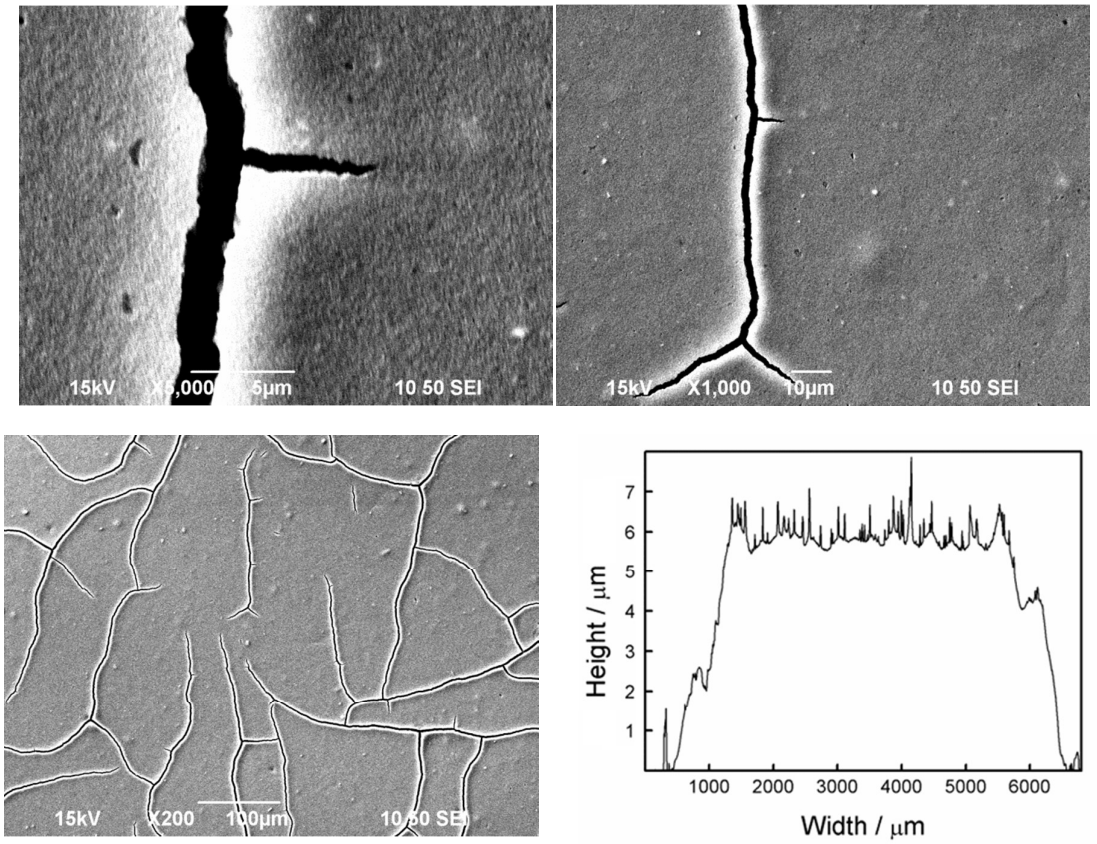

Figure 2. SEM micrographs of a TiO_2 electrode screen printed with the diluted Paste C at different magnifications together with profilometer data (bottom right).

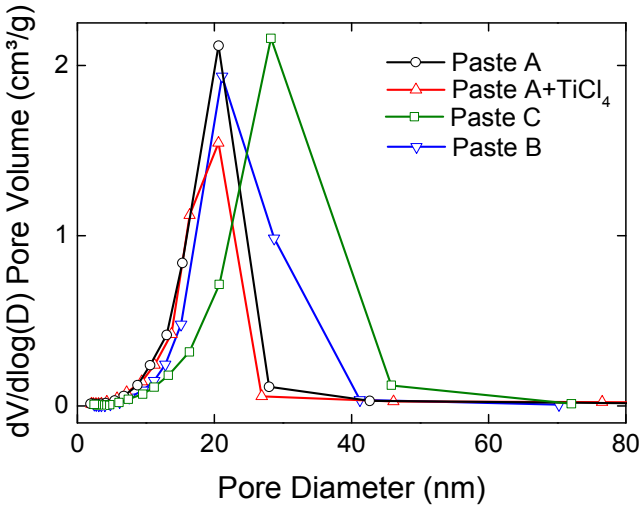

Figure 3. Pore-size distributions for the different mesoporous TiO_2 samples

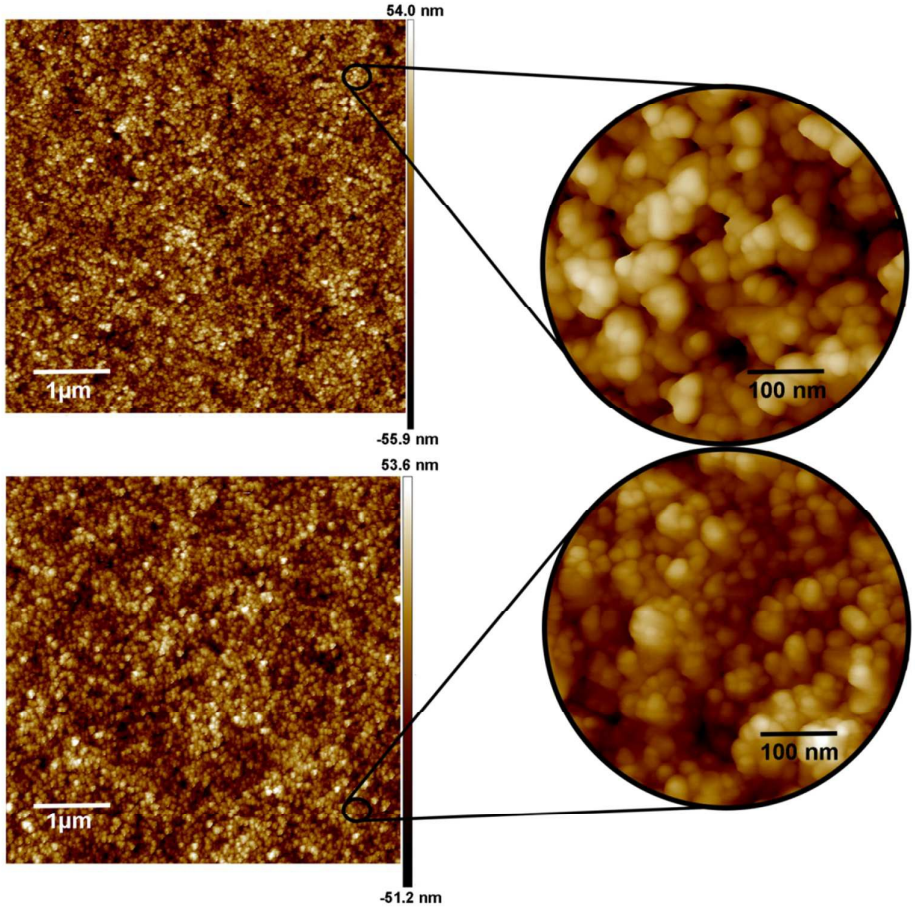

Figure 4. AFM images of TiO_2 electrodes a) top images: before $TiCl_4$ treatment at 5µm scale and 500 nm scale and b) bottom images: after $TiCl_4$ treatment (right) at 5µm scale and 500 nm scale.

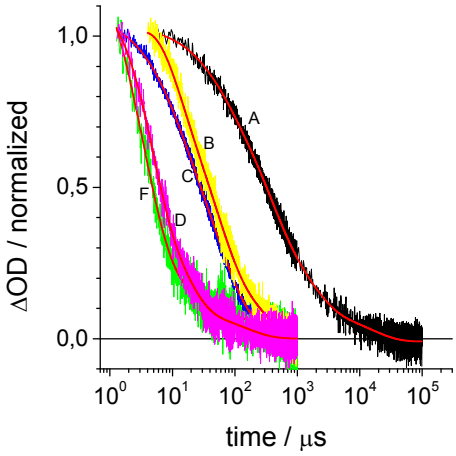

Figure 5. Transient absorption kinetics of D35-sensitized TiO_2 electrodes employing different cobalt(II) complexes A) inert solution; B) $Co^{II}(dclphen)_3$; C) $Co^{II}(dclbpy)_3$; D) $Co^{II}(dMeObpy)_3$ and F) $Co^{II}(bpy)_3$. The electrolyte used contained 0.22M Co^{II}, 0.1M $LiClO_4$ and 0.2M TBP in a 60:40 mixture of acetonitrile and ethylene carbonate.

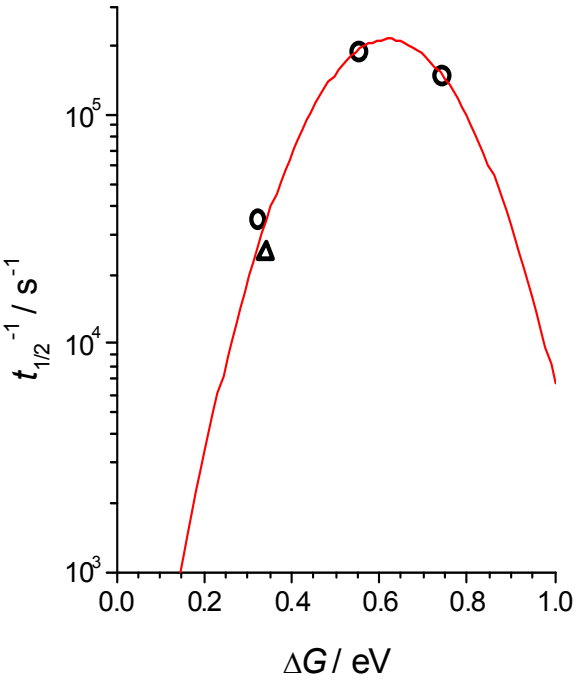

Figure 6. Semilogarithmic plot of the inverse of the halftime for the reaction between oxidized D35 and the cobalt redox mediators. The fitted curve represents the Marcus theory (eq. 1) for the regeneration kinetics using a solution of 0.22 M Co^{II}, 0.1 M $LiClO_4$ and 0.2 M TBP in a 60:40 mixture by weight of acetonitrile and ethylene carbonate. Bipyridine based cobalt complexes are represented by ● and $Co^{II}(dclphen)_3$ is represented by ▲.

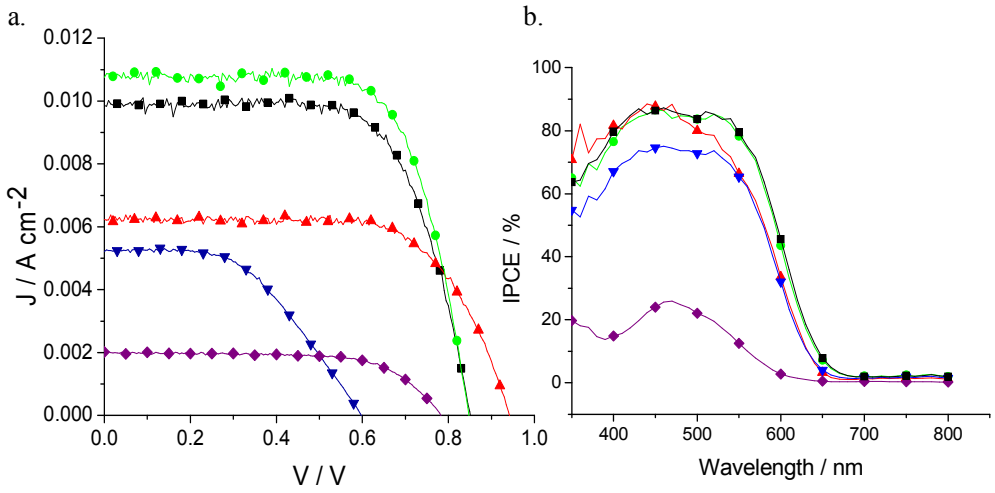

Figure 7. a) Current density vs applied potential curves under AM1.5G illumination for DSSCs based on the different cobalt complexes as electrolyte redox mediators, b) Spectra of incident photon-to-current efficiency (IPCE) for DSSCs based on the different mediators. The traces symbolize ▲ $Co^{II/III}(dclbpy)_3$, ▼ $Co^{II/III}(dMeO\text{-}bpy)_3$, ♦ $Co^{II/III}(dclphen)_3$, ● and ■ $Co^{II/III}(bpy)_3$ electrolytes . A solution of 40 wt% ethylene carbonate + 60 wt% acetonitrile was used as solvent for the electrolyte. For ● $Co^{II/III}(bpy)_3$ pure acetonitrile was used.

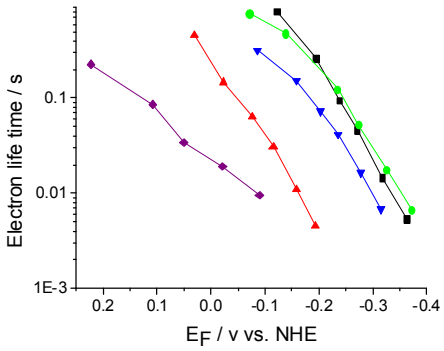

Figure 8. Electron lifetime as a function of the quasi-Fermi level of TiO_2 under open-circuit conditions for DSSCs sensitized with D35 containing different cobalt-based electrolytes. The traces symbolize ▲ $Co^{II/III}(dclbpy)_3$, ▼ $Co^{II/III}(dMeO\text{-}bpy)_3$, ♦ $Co^{II/III}(dclphen)_3$, ● $Co^{II/III}(bpy)_3$ and ■ $Co^{II/III}(bpy)_3$ electrolytes. A solution of 40 wt% ethylene carbonate + 60 wt% acetonitrile was used as solvent for the electrolytes. For ● $Co^{II/III}(bpy)_3$ pure acetonitrile was used.